Title

Essential Role of ELOVL4 Protein in Very Long Chain Fatty Acid Synthesis and Retinal Function*

Journal

Journal of Biological Chemistry, 287(14)

ISSN

0021-9258

Authors

Harkewicz, Richard
Du, Hongjun
Tong, Zongzhong
et al.

Publication Date

2012-03-01

DOI

10.1074/jbc.m111.256073

Peer reviewed

THE JOURNAL OF BIOLOGICAL CHEMISTRY VOL. 287, NO. 14, pp. 11469–11480, March 30, 2012

Essential Role of ELOVL4 Protein in Very Long Chain Fatty Acid Synthesis and Retinal Function*

Received for publication, April 29, 2011, and in revised form, December 22, 2011 Published, JBC Papers in Press, December 24, 2011, DOI 10.1074/jbc.M111.256073

Richard Harkewicz[‡1], Hongjun Du[§¶‖1], Zongzhong Tong[§], Hisham Alkuraya[§], Matthew Bedell[§], Woong Sun[§], Xiaolei Wang[§], Yuan-Hao Hsu[‡], Julian Esteve-Rudd[‡‡], Guy Hughes[§], Zhiguang Su[¶], Ming Zhang[¶], Vanda S. Lopes[‡‡], Robert S. Molday[§§], David S. Williams[‡‡2], Edward A. Dennis[‡3], and Kang Zhang[§¶4]**

From the [‡]Department of Chemistry and Biochemistry, Department of Pharmacology, and School of Medicine and [§]Department of Ophthalmology, Shiley Eye Center, and Institute for Genomic Medicine, University of California, San Diego, La Jolla, California 92093, [¶]Molecular Medicine Research Center and Department of Ophthalmology, West China Hospital, Sichuan University, Chengdu 610041, China, [‖]Department of Ophthalmology, Xijing Hospital, Fourth Military Medical University, Xi'an 710032, China, [**]Tong Ren Eye Hospital, Beijing 100730, China, [‡‡]Jules Stein Eye Institute and Departments of Ophthalmology and Neurobiology, UCLA School of Medicine, Los Angeles, California 90095, and [§§]Departments of Biochemistry and Molecular Biology and Ophthalmology and Visual Sciences, Centre for Macular Research, University of British Columbia, Vancouver, British Columbia V6T 1Z3, Canada

Background: Phospholipids containing very long chain polyunsaturated fatty acids (VLC-PUFAs) are enriched in retina.
Results: Specific ELOVL4 rod or cone photoreceptor conditional knock-outs cause decreases in retinal VLC-PUFAs.
Conclusion: ELOVL4 is critical for the synthesis of phosphatidylcholine-containing *sn*-1 VLC-PUFAs and vision.
Significance: ELOVL4 mutations are implicated in Stargardt disease, a type of juvenile macular degeneration.

Very long chain polyunsaturated fatty acid (VLC-PUFA)-containing glycerophospholipids are highly enriched in the retina; however, details regarding the specific synthesis and function of these highly unusual retinal glycerophospholipids are lacking. Elongation of very long chain fatty acids-4 (ELOVL4) has been identified as a fatty acid elongase protein involved in the synthesis of VLC-PUFAs. Mutations in *ELOVL4* have also been implicated in an autosomal dominant form of Stargardt disease (STGD3), a type of juvenile macular degeneration. We have generated photoreceptor-specific conditional knock-out mice and used high performance liquid chromatography-mass spectrometry (HPLC-MS) to examine and analyze the fatty acid composition of retinal membrane glycerophosphatidylcholine and glycerophosphatidylethanolamine species. We also used immunofluorescent staining and histology coupled with electrophysiological data to assess retinal morphology and visual response. The conditional knock-out mice showed a significant decrease in retinal glycerophospholipids containing VLC-PUFAs, specifically contained in the *sn*-1 position of glycerophosphatidylcholine, implicating the role of *Elovl4* in their synthesis. Conditional knock-out mice were also found to have abnormal accumulation of lipid droplets and lipofuscin-like granules while demonstrating photoreceptor-specific abnormalities in visual response, indicating the critical role of *Elovl4* for proper rod or cone photoreceptor function. Altogether, this study demonstrates the essential role of ELOVL4 in VLC-PUFA synthesis and retinal function.

Stargardt disease (STGD[5]; fundus flavimaculatus) is the most common hereditary form of macular dystrophy and accounts for 7% of all retinal dystrophies (estimated incidence, 1:10,000) (1, 2) with patients presenting decreased central vision often in the first or second decade of life. Ophthalmoscopically, STGD is characterized by bilateral atrophic changes in the macula, degeneration of underlying retinal pigment epithelium (RPE), and the presence of prominent yellowish flecks in the posterior pole. STGD can be inherited as either a recessive or dominant trait. A dominant locus has been mapped to chromosome 6q14 (STGD3; MIM 600110), and elongation of very long chain fatty acids-4 (*ELOVL4*) (GenBank™ accession number AF277094; MIM 605512) was identified as the causative gene (3, 4).

The *ELOVL4* gene encodes a membrane protein consisting of 314 amino acids that is predominantly expressed in rod and cone photoreceptors in the retina and to a lesser extent in the brain (4). The ELOVL4 protein is characterized by five putative transmembrane segments, a single dioxy iron binding motif (H*XX*HH), which is essential for enzymatic activity (5, 6), and a

* This work was supported, in whole or in part, by National Institutes of Health Grants EY014428, EY018660, and EY019270 (to K. Z.) and EY07042 (to D. S. W.) from the NEI and Grant U54 GM069338, a LIPID MAPS large scale collaborative "glue" grant from the NIGMS(to E.A.D.).

[1] Both authors contributed equally to this work.

[2] Supported by Research to Prevent Blindness Jules and Doris Stein Professorship.

[3] To whom correspondence may be addressed: Depts. of Chemistry and Biochemistry and Pharmacology, University of California, San Diego, 9500 Gilman Dr., La Jolla, CA 92093-0601. Tel.: 858-534-3055; E-mail: edennis@ucsd.edu.

[4] Supported by the National Basic Research Program of China (973 Program, Grant 2011CB510200), a Veterans Affairs merit award, Research to Prevent Blindness, a Burroughs Wellcome Fund clinical scientist award in translational research,and the King Abdulaziz City for Science and Technology (KACST). To whom correspondence may be addressed: Inst. for Genomic Medicine, University of California, San Diego, 9500 Gilman Dr., La Jolla, CA 92093-0838. Tel.: 858-246-0823; Fax: 858-246-0961; E-mail: kang.zhang@gmail.com.

[5] The abbreviations used are: STGD, Stargardt disease; RPE, retinal pigment epithelium; ELOVL, elongation of very long chain fatty acids; VLC-PUFA, very long chain polyunsaturated fatty acid; ER, endoplasmic reticulum; PC, glycerophosphatidylcholine; PE, glycerophosphatidylethanolamine; GIA sPLA$_2$, Group IA secreted phospholipase A$_2$; ERG, electroretinogram; *ELOVL4*, human gene; *Elovl4*, mouse gene; ELOVL4, protein; MRM, multiple reaction monitoring; FRT, flippase recognition target; DHA, docosahexaenoic acid.

carboxyl-terminal dilysine motif (K*X*K*XX*) necessary for endoplasmic reticulum (ER) retention (7–9). Three alleles have been identified as the cause for STGD3, each possessing a mutation in the last exon (exon 6) of *ELOVL4*. These mutations include a 5-bp deletion (790–794delAACTT), two 1-bp deletions (789delT and 794delT), and a single transversion (C-to-G at position 810) resulting in a premature stop codon (Y270X) (4, 10, 11). Each *ELOVL4* mutation results in a truncated protein with a carboxyl-terminal dilysine motif absent, leading to loss of retention in the ER; very long chain polyunsaturated fatty acid (VLC-PUFA) biosynthesis takes place in the ER (12). By definition, a VLC-PUFA has 24 or more carbon atoms and from four to six methylene-interrupted *cis* double bonds (18, 31). When co-expressed in cell transfection studies, mutant ELOVL4 was found to exert a dominant negative effect on the wild type protein, resulting in the mislocalization of the wild type protein to non-ER juxtanuclear aggregates (13–15).

Based on the homology of ELOVL4 to the ELO family of yeast proteins as well as other members of the mammalian ELOVL family and the strong conservation of ELOVL4 between vertebrate species, ELOVL4 was predicted to play an essential role in the biosynthesis of VLC-PUFAs (4, 16–21). Cameron *et al.* (22) examined the specific elongase activity of ELOVL4 using homozygous *Elovl4* Y270X knock-in and homozygous *Elovl4* knock-out mice and observed that mice lacking functional ELOVL4 died perinatally due in part to dehydration from a faulty skin permeability barrier. The skin of both the homozygous mutant and the knock-out mouse was deficient in glycerophospholipids containing fatty acids 26 carbon atoms or longer in chain length, implicating ELOVL4 in their biosynthesis. Agbaga *et al.* (23) confirmed the metabolic function of ELOVL4, demonstrating that it is an elongase protein involved in the synthesis of VLC-PUFAs, particularly those of the polyunsaturated C_{28}–C_{38} *n*-3 variety (Fig. 1, *A* and *B*). This elongase activity was studied using an *in vitro* gain-of-function approach by expressing the mouse ELOVL4 protein in rat cardiomyocytes and human RPE (23). Although ELOVL4 appears to be expressed only in tissues in which VLC-PUFAs are observed (24) and it has been noted that the retina is particularly enriched in VLC-PUFAs (23, 25, 26), no study to date has confirmed that ELOVL4 is indeed responsible for the biosynthesis of VLC-PUFAs in the retina. However, it has recently been reported that the epidermal expression of an *Elovl4* transgene rescues neonatal lethality of homozygous Stargardt disease-3 mice (27). In the present work, we have generated separately retinal rod- and cone-specific homozygous *Elovl4* knock-out mice and investigated membrane glycerophospholipid fatty acid composition, retinal morphology, and physiology. Furthermore, we examined the VLC-PUFA composition in retinal membrane-intact glycerophospholipids and demonstrated that the deficiency is specific to glycerophosphocholine (PC) species. Our results indicate that ELOVL4 is essential for VLC-PUFA synthesis as well as retinal functions.

EXPERIMENTAL PROCEDURES

Generation of Photoreceptor-specific Conditional Knock-out (cKO) Mice—The DNA fragment that contained exon 2, exon 3, and the flanking region of *Elovl4* was cloned from a 129s7/AB2.2 bacterial artificial chromosome duplicate by homologous recombination (28). The FRT-flanked neomycin cassette and the two LoxP sites were inserted into intron 1 and intron 2 through subcloning, whereas the two homologous genomic fragments, which flanked the cassette and thus mediated the homologous recombination, replaced exons 2 and 3 in the endogenous *Elovl4* gene. A herpes simplex virus thymidine kinase gene outside of the 3′ homologous arm and from the backbone of the vector was used as a negative selection marker in subsequent screenings (Fig. 2*A*). The final gene-targeting construct was then electroporated into mouse embryonic stem (ES) cells derived from 129/SvEv embryonic stem cells (AB2.2, Stratagene) and cultured in the presence of G418 (positive selection) or ganciclovir (negative selection). Genomic DNA was extracted from transfected ES clones to identify homologous recombination in which the targeted endogenous exons 2 and 3 were replaced with the FRT-Neo-loxp cassette and the negative selection marker (thymidine kinase) was lost using a polymerase chain reaction (PCR) and Southern blotting. A positive clone (clone 7; Fig. 2*B*) was injected into mouse blastocysts derived from a C57B/6 background to generate chimeric mice. The chimeric mice were then bred with wild type C57B/6 (outbred) mice to produce heterozygous specimens that were then genotyped by PCR, incorporating an Elovl4-loxp2-gt-L/Elovl4-loxp2-gt-R primer. Heterozygous agouti mice were cross-bred to generate floxed homozygotes. The homozygous *Elovl4* lines having floxed alleles were cross-bred with specimens having photoreceptor-specific Cre-expressing lines to achieve photoreceptor-specific gene inactivation. The cone- or rod-specific Cre mice (29, 30) were provided by Dr. Yun Le. All animal experiments followed the guidelines of the Association for Research in Vision and Ophthalmology Statement for the use of animals in ophthalmic and vision research and were approved by the Animal Care Committee of the University of California, San Diego.

Extraction of Retinal Glycerophospholipids—The removed retinal tissue samples were placed in a 10-ml borosilicate glass tube to which 2 ml of ice-cold dichloromethane/methanol (2:1, v/v) was added, and then a probe sonicator was used to pulverize the tissue. The tube was then capped and vigorously shaken for 1 h at room temperature. Two milliliters of water was then added, and the contents were vortexed at maximum speed for 1 min. The tube and contents were then centrifuged (5000 × *g* for 2 min), and the lower, separated phase was removed and placed in another glass tube. This lower liquid phase was stored at −80 °C until further analysis at which time its contents were evaporated to dryness with a stream of argon gas, and the remaining contents was resuspended in 100 μl of high performance liquid chromatography (HPLC) buffer solution A.

Normal Phase Liquid Chromatography of Retinal Extracts—HPLC was carried out using two Shimadzu (Columbia, MD) LC-10AD high performance chromatography pumps interfaced with a Shimadzu SCL-10A controller. The extracted retinal samples were injected onto the liquid chromatography analytical column using a Leap Technologies (Carrboro, NC) PAL autosampler. Normal phase separation was achieved using a 2.0 × 250-mm Phenomenex (Torrance, CA) silica column (Phenomenex catalogue number 00G-4274-B0) held at 40 °C. Buffer solution A consisted of isopropanol, hexane, 100 mM

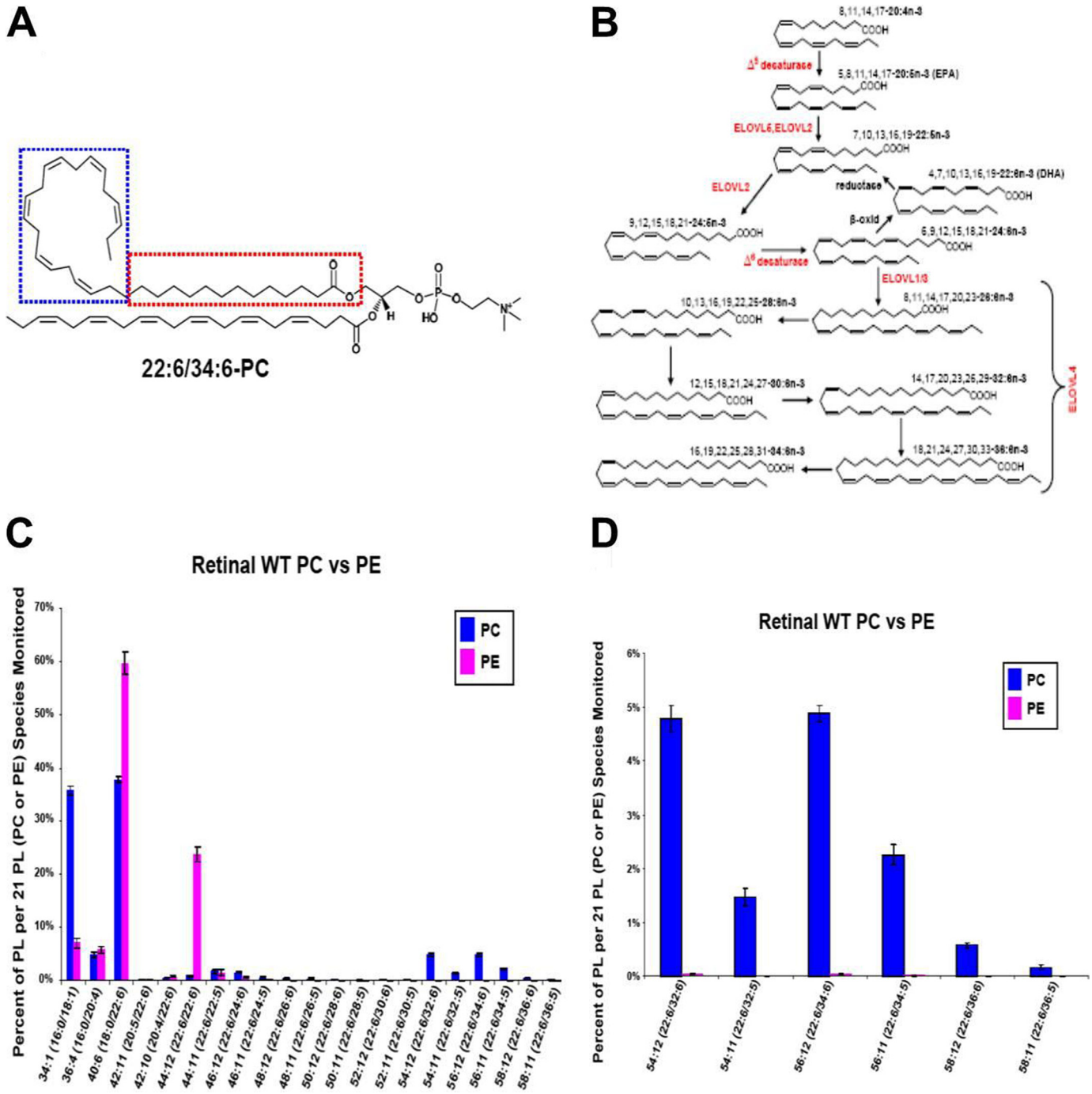

FIGURE 1. **Analysis of extracted phospholipids from retinas.** *A*, anatomy of a typical very long chain polyunsaturated PC lipid molecule found in retinal extracts. A VLC-PUFA is located on the *sn*-1 position of the molecule, whereas DHA occupies its *sn*-2 position. These PC species containing VLC-PUFA are unique in that the proximal carboxylic region (*red box*) is composed of some 14+ saturated carbon bonds, whereas the distal region (*blue box*) contains up to six methylene-interrupted *cis* double bonds. Such species have the length to occupy both halves of a lipid bilayer and would provide quite different physical properties to each side. *B*, a combination of various desaturase and elongase enzymes is involved in the synthesis of VLC-PUFAs based on the revised pathway of Sprecher *et al.* (44). The VLC-PUFA series containing six double bonds is shown; a series with five double bonds is similarly formed. *C*, distribution of PC *versus* PE species observed in WT mouse retinal extracts. Note that the PC species containing VLC-PUFA (those having an *sn*-1 fatty acid 32–36 carbon atoms in length) account for over 10% of the PC species monitored; this is shown in greater detail in *D*. By comparison, the PE species observed in retinal extracts contain hardly any of these VLC-PUFA species. Data shown in *C* and *D* are representative of six independent analyses (each retina from three mice).

ammonium acetate (aqueous) (55:40:5, v/v/v); buffer solution B consisted of isopropanol, hexane, 100 mM ammonium acetate (aqueous) (50:40:10, v/v/v). Gradient chromatographic elution was achieved using 100:0 A/B at 0 min and linearly ramped to 25:75 A/B by 25 min, ramped to 0:100 A/B by 26 min, and held there until 35 min. A/B was ramped back to 100:0 by 37 min and held there until 55 min for column equilibration. The buffer flow rate was 0.3 ml/min. Separation optimization was achieved using PC and glycerophosphoethanolamine (PE) standards. For each sample analyzed, 40 μl of sample was injected onto the column. The HPLC effluent was coupled to a mass spectrometer for further analysis.

All PC and PE lipid standards used for HPLC and mass spectrometry (MS) optimization were purchased from Avanti Polar Lipids (Alabaster, AL). Solvents used for HPLC were of chromatography grade and purchased from OmniSolv (Gibbstown, NJ). Ammonium acetate used as an HPLC additive was purchased from Sigma-Aldrich.

Mass Spectrometry—All mass spectrometric analyses were performed using an AB Sciex (Foster City, CA) 4000 QTrap hybrid quadrupole linear ion trap mass spectrometer equipped with a Turbo V ion source. Acetate anion adducts of the PC species and deprotonated anions of the PE species were formed by operating the ion source in negative electrospray ionization mode using the following settings: curtain gas, 10 p.s.i.; nebulizer gas pressure, 20 p.s.i.; heater gas pressure, 20 p.s.i.; ion spray voltage, −4500 V; temperature, 500 °C. The mass spectrometer was operated in multiple reaction monitoring (MRM) mode using the following settings: declustering potential, −120 V; entrance potential, −15 V; collision cell exit potential, −15 V; collision energy, −55 V. An MRM method was created and used that included precursor ion mass/acyl chain fragment pairs for PC and PE species monitored. AB Sciex mass spectrometer software (Analyst 1.5.1) was used to analyze the collected sample data.

In Vitro Group IA Secreted Phospholipase A_2 (GIA $sPLA_2$) Assay of Retinal Glycerophospholipids—The *in vitro* GIA $sPLA_2$ assay used in this work was modified from assays described previously (31, 32). Briefly, extracted retinal glycerophospholipids from wild type (WT) mice (as described above) were dried under argon immediately prior to preparing a mixed micelle buffer solution for the $sPLA_2$ assay. The mixed micelle buffer was composed of 400 μM Triton X-100, 50 mM Tris, pH 8.0, and 5 mM $CaCl_2$. The dried retinal lipids were dissolved in 500 μl of the mixed micelle buffer, incubated at 40 °C for 2 h, and vortexed every 20 min for a period of 30 s. This mixture was then initiated by adding 2 μl of (0.8 mg/ml) GIA $sPLA_2$ into the mixed micelle substrate and incubated at 40 °C for an additional 2 h. A control was prepared that was identical to the above sample except that no $sPLA_2$ was added. The glycerophospholipids from the two samples were then extracted and analyzed using HPLC-MS as described above. The GIA $sPLA_2$ was purified from cobra venom (*Naja naja naja*) as described previously (33).

Immunofluorescent Staining and Histology—All eye samples were dissected from adult mice, fixed with 4% paraformaldehyde for 2 h at 4 °C, and cryoprotected in a 30% sucrose solution. Samples were frozen and sectioned (16 μm) on a cryostat. For immunohistochemistry, the sections were incubated with blocking solution (3% BSA and 0.3% Triton X-100 in PBS) for 30 min followed by overnight incubation with primary antibodies at 4 °C. Primary antibodies used were Rhodopsin (1:200; Millipore), S-Cone (1:200; Santa Cruz Biotechnology), and ROM1 (a gift from Dr. R. Molday of University of British Columbia). After rinses with PBS, sections were incubated with Alexa Fluor 488-conjugated anti-mouse antibody (1:1000; Millipore) and Alexa Fluor 555-conjugated anti-goat antibody (1:1000; Millipore) for 30 min at room temperature. Sections were counterstained with DAPI and mounted, and the images were captured using an Olympus FV1000 confocal microscope.

Electron Microscopy—Eyes from 15-month-old wild type control mice and 15-month-old mutant mice were enucleated, and their anterior segments were quickly dissected away while immersed in primary fixative (2% glutaraldehyde + 2% formaldehyde in 0.1 M cacodylate buffer, pH 7.4). The resulting eyecups were maintained in primary fixative for ~24 h, then post-fixed in 1% OsO_4 in the same buffer, dehydrated, and embedded in Epon. Semithin sections were stained with toluidine blue and imaged by light microscopy. Ultrathin sections were stained with uranyl acetate and lead citrate and imaged by transmission electron microscopy.

Electroretinography—Electroretinograms (ERGs) were obtained from adult mice in a full-field dome using methods similar to those in clinical practice and using stimuli comparable with standards cited by the International Society for Clinical Electrophysiology of Vision. The mice were dark-adapted overnight and prepared for recording the next day under dim red light conditions. ERG recordings were conducted as described previously (13). In brief, anesthesia was induced using an intraperitoneal injection of a mixture of ketamine (90 mg/kg) and xylazine (9 mg/kg) in saline solution. Pupils were dilated using a mixture of tropicamide (1%) and phenylephrine (2.5%). Proparacaine (0.5%) was used as a topical anesthetic to minimize blinking. Mice were then placed on a heating pad in a Ganzfeld bowl stimulator on a sliding table. ERGs were recorded using a looped thin stainless steel wire to make contact with the corneal surface through a thin layer of Genteal Tear Gel (Novartis Pharmaceuticals). Needle electrodes placed in the lower lip and tail served as reference and ground leads, respectively. Amplification with a Grass 15LT external amplifier (at 0.3–300 Hz without notch filtering), stimuli presentation, and data acquisition were programmed and performed using the VERIS 6.0.9 Science software system (Electro-Diagnostic Imaging, Inc., Redwood City, CA). Single flashes (0.05-ms duration (0.0084 Candela−s total) with 10-s intervals for 10 counts in scotopic testing, 1.0-ms duration (2.686 Candela−s per square meter total) with 10-s intervals for 10 counts in mixed testing, and 1.0-ms duration (2.686 Candela−s per square meter total) with 100-ms intervals in photopic flicker testing) were obtained under both dark-adapted conditions and light-adapted conditions. For photopic ERG responses, mice were light-adapted for a minimum of 10 min prior to recording. Mice were placed on a heating pad and visually observed until the effects of the anesthetics had diminished entirely.

RESULTS

Generation of Rod- or Cone-specific Elovl4 Knock-out Mice—After the *Elovl4* gene-targeting construct was electroporated into mouse ES cells and cultured in the presence of G418 (positive selection) and ganciclovir (negative selection), genomic DNA was extracted for Southern blotting analysis with the external probe (Fig. 2*A*, *purple bar*). Of eight transfected ES clones, our result demonstrated the presence of the mutant construct as indicated by the 4.7-kb band (Fig. 2*B*, *lane 7*). After cross-breeding FRT-Neo-loxP mice with ACTB-FLP mice to remove the neomycin marker, genomic DNA was obtained from mouse lines for PCR genotyping to confirm the creation of a conditional floxed *Elovl4* allele (Fig. 2*C*). Homozygous *Elovl4*

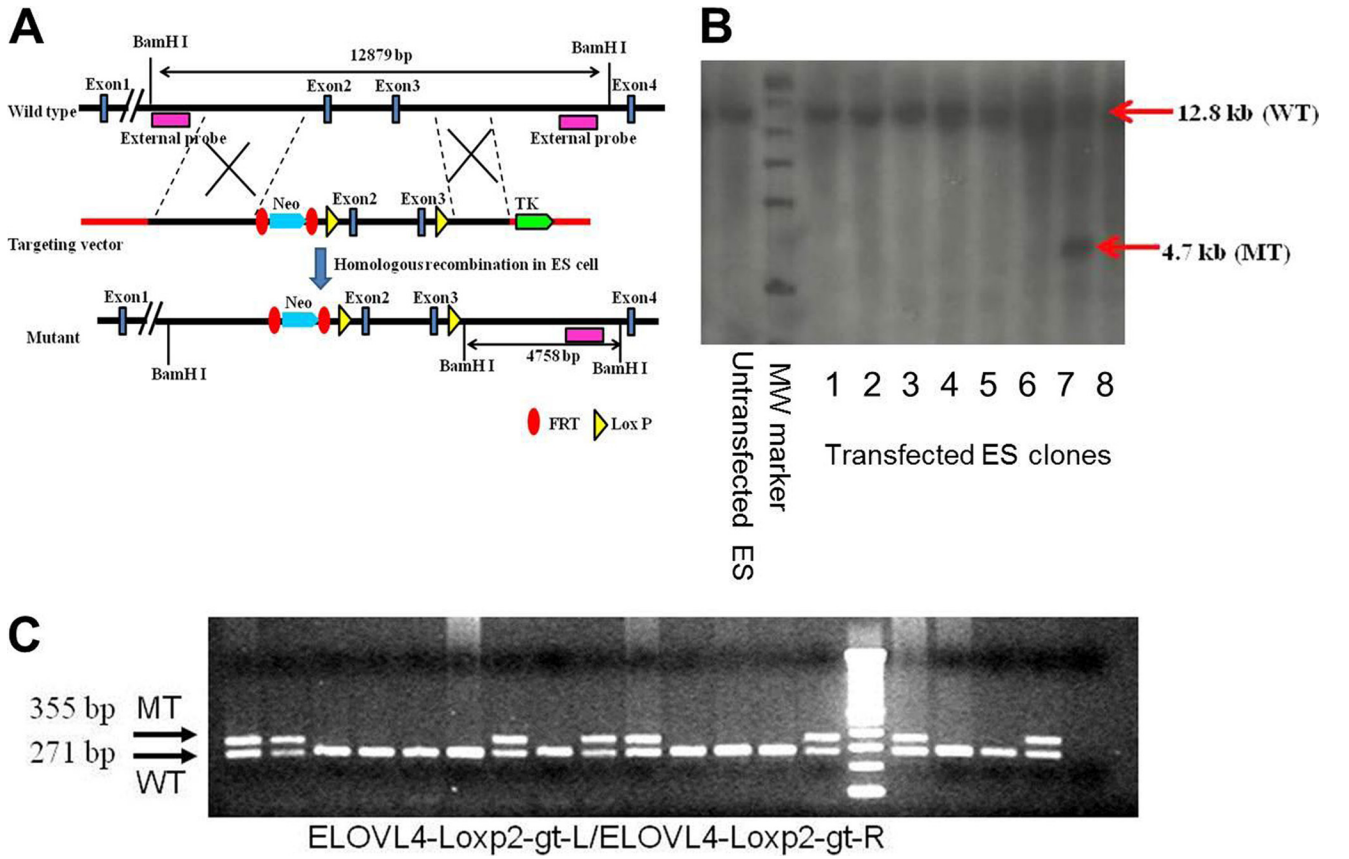

FIGURE 2. ***Elovl4* cKO construct.** *A*, the schematic diagram of the *Elovl4* locus and targeting construct. An FRT-flanked neomycin (*Neo*) cassette positive selection marker was inserted into intron 1. Exons 2 and 3 were flanked by two LoxP sites. There is a herpes simplex virus thymidine kinase (*TK*) counterselection cassette in the 5′-end of the vector. The wild type band expected from BamHI digestion is 12.8 kb; the mutant (*MT*) band is 4.7 kb. *B*, Southern blot analysis of ES cell genomic DNA after digestion with BamHI and hybridization with 3′ external probes. *Left* of the molecular weight marker is genomic DNA from untransfected ES cells, and *lanes 1-8* are genomic DNA from clones 1–8 with transfected targeting construct. *C*, PCR genotyping of agouti mouse genomic DNA. A single 271-bp fragment appears in the case of wild type mice, and an additional 355-bp fragment appears in the case of heterozygous mutant mice.

lines with floxed alleles were then cross-bred with mice having photoreceptor-specific Cre-expressed lines to achieve the photoreceptor-specific *Elovl4* gene knock-out specimen.

Analysis of Retinal Extract Glycerophospholipids—Extracts obtained from WT mouse retina were analyzed for a total of 21 different PC and PE molecular species (42 total), including those containing both five- and six-double bond VLC-PUFA acyl chains; these results are shown in Fig. 1, *C* and *D*. An initial survey revealed no significant glycerophospholipid species containing VLC-PUFA with fewer than five or more than six double bonds present (data not shown), so these species were not monitored in subsequent retinal surveys. An HPLC-MS MRM method was created that included precursor anion mass/acyl chain fragment anion mass MRM pairs specific for these 21 PC and PE species. The relative percent abundance shown in Fig. 1, *C* and *D*, was determined by integrating the area under each MRM defined peak, separately summing for the PCs and PEs, and calculating the percentage of each molecular species comprising the PC and PE totals; this assumes that ionization and fragmentation efficiencies for the different molecular species are similar. Comparing the PCs with the PEs, in addition to showing a difference in the distribution of the various species, these results also show that the vast majority of the glycerophospholipids containing VLC-PUFAs are restricted to the PCs with those containing C_{32}–C_{36} VLC-PUFAs comprising over 10% of the 21 species monitored. These results are the average of six independent analyses (each retina from three mice) and are in agreement with earlier studies (34, 35).

An absolute quantitative measurement (*e.g.* pmol amount/mg of retinal tissue) of the PC and PE species monitored was not feasible as no deuterium-labeled internal standards are currently commercially available for any of the glycerophospholipids containing VLC-PUFA acyl chains, and it is for this reason that we report relative abundances in our current work. However, using accurately measured primary standards for some of the more abundant shorter chain PC and PE species (*e.g.* 16:0/18:1), we estimated the total PC abundance to be ~5-fold higher compared with the total PE abundance.[6]

To confirm an earlier study (34) showing that VLC-PUFA acyl species were contained almost exclusively on the *sn*-1 position of retinal PCs with docosahexaenoic acid (DHA; 22:6*n*-3)

[6] Using commercially available 16:0/18:1-PC and 16:0/18:1-PE standards, each with accurately known concentrations, we observed that equal absolute quantities of each standard produced approximately the same intensity mass spectral monitoring signal peak (MRM pair: precursor anion mass/acyl chain fragment anion mass). Thus, for our retinal samples, signal intensities obtained from PC and PE species having the same two acyl chain moieties could be used to estimate an absolute -fold difference, allowing us to estimate the total PC abundance to be approximately 5-fold higher compared with the total PE abundance.

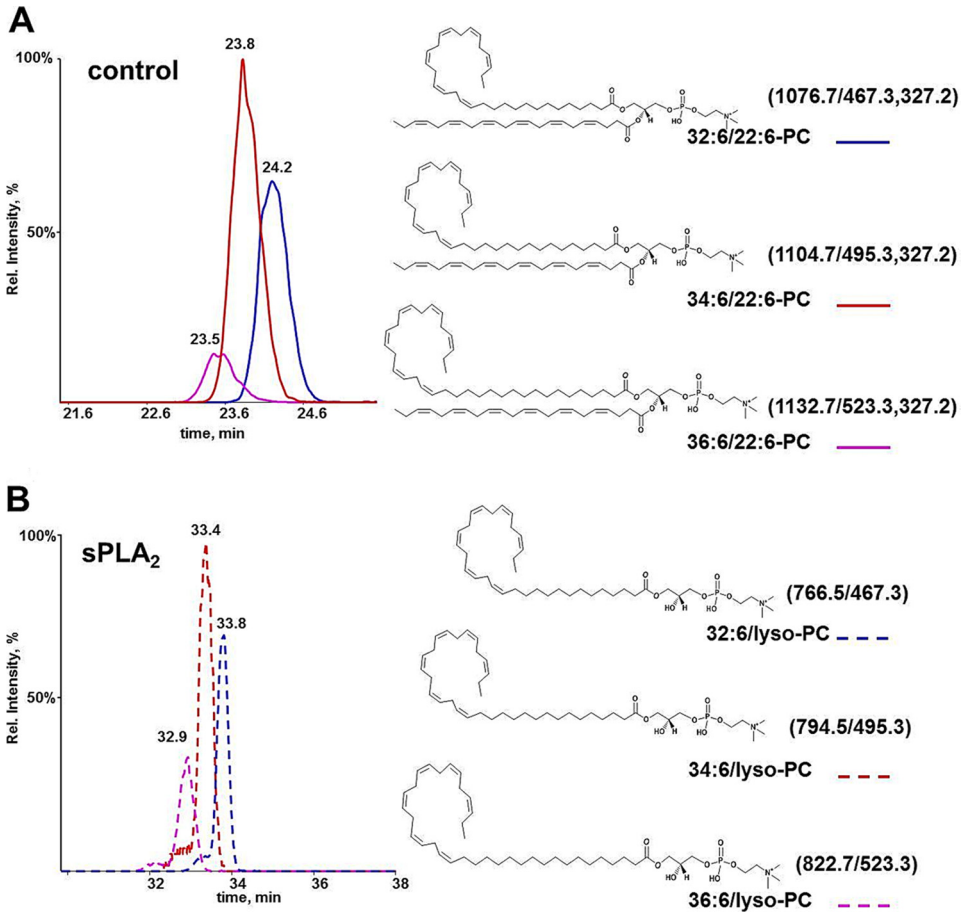

FIGURE 3. ***In vitro* GIA sPLA$_2$ assay of retinal glycerophospholipids.** The HPLC-MS MRM chromatogram results for extracted mouse WT retinal glycerophospholipid control (*A*) and GIA sPLA$_2$-treated sample (*B*) show that the VLC-PUFAs are located exclusively on the *sn*-1 position of retinal PCs. The chemical structures for C_{32}–C_{36} VLC-PUFA-containing PCs are shown along with their acetate adduct anion precursor masses and the *sn*-1 and *sn*-2 acyl chain fragment masses (MRM pairs). Their corresponding lyso-PC analogs, the result of sPLA$_2$ cleaving the *sn*-2-located DHA, are also shown. *Rel.*, relative. *Error bars* represent S.E.

occupying the *sn*-2 position, an *in vitro* GIA sPLA$_2$ assay was carried out in the current work, and the results are shown in Fig. 3. An HPLC-MS MRM method was created that included precursor acetate adduct anion mass/acyl chain fragment anion mass MRM pairs as well as their corresponding lyso analogs (result of cleaving the VLC-PUFA or the DHA acyl chain from these PCs). The same HPLC-MS-MRM method was used to monitor both the control (Fig. 3*A*) and the sPLA$_2$-treated (Fig. 3*B*) samples. As expected, PC species containing both the intact VLC-PUFA and the DHA acyl chains were observed in the control sample, and these were not observed in the sPLA$_2$-treated sample. The sample treated with the sPLA$_2$ showed the presence of VLC-PUFA-containing lyso-PC species. Because sPLA$_2$ is specific for cleaving the *sn*-2 acyl chain (36), these results confirm that the VLC-PUFAs are indeed located on the *sn*-1 position of PC. Lyso-PC-containing DHA was also monitored; however, its minimal increase in the sPLA$_2$-treated sample would imply that it was not located on the *sn*-2 position of the VLC-PUFA-containing PCs.

Next, the retinal extracts from both mouse Rod-cKO and Cone-cKO samples were assayed for the 21 PC species and compared with mouse WT samples. The relative percentages of PC species (Fig. 4, *A* and *B*) were determined, and differences in each PC molecular species among Rod-cKO *versus* WT and Cone-cKO *versus* WT are shown as a ratio difference in Fig. 4*C*. Those species falling on or near the *heavy dashed horizontal bar* at a ratio equal to 1 are approximately the same among the cKOs *versus* WT (*e.g.* 16:0/18:1 and 18:0/22:6), those *above* the *bar* are higher in the cKOs *versus* WT (*e.g.* 22:6/22:6 and 22:6/22:5), and those *below* the *bar* are lower in the cKOs *versus* WT (*e.g.* 22:6/34:6 and 22:6/36:6). Fig. 4*D* shows the proposed synthetic pathway shown earlier in Fig. 1*B*; highlighted in *blue* are those species higher in the Rod-cKO compared with WT, whereas highlighted in *red* are those species lower in the Rod-cKO compared with WT.

Retinal Morphology in Photoreceptor-specific Elovl4 Conditional Knock-out Mice—Immunohistochemistry and confocal microscopy carried out on the frozen sections of the retinas of 3–5-month old WT, Rod-cKO, and Cone-cKO mice show similar retinal morphology in both photoreceptor-specific cKOs compared with WT (Fig. 5, *A*–*F*). Gross morphology was normal (Fig. 6, *A* and *B*), although there was a mild loss of photoreceptor cells in the Rod-cKO retinas. Counts of nuclei (500 μm either side of the optic nerve head in dorsoventral sections) revealed that 10-month-old Rod-cKO mutants had eight rows of nuclei, and 15-month-old Rod-cKO mutants had seven rows of nuclei in comparison with nine rows of nuclei for 15-month-old normal controls. The disk membranes of the rod outer seg-

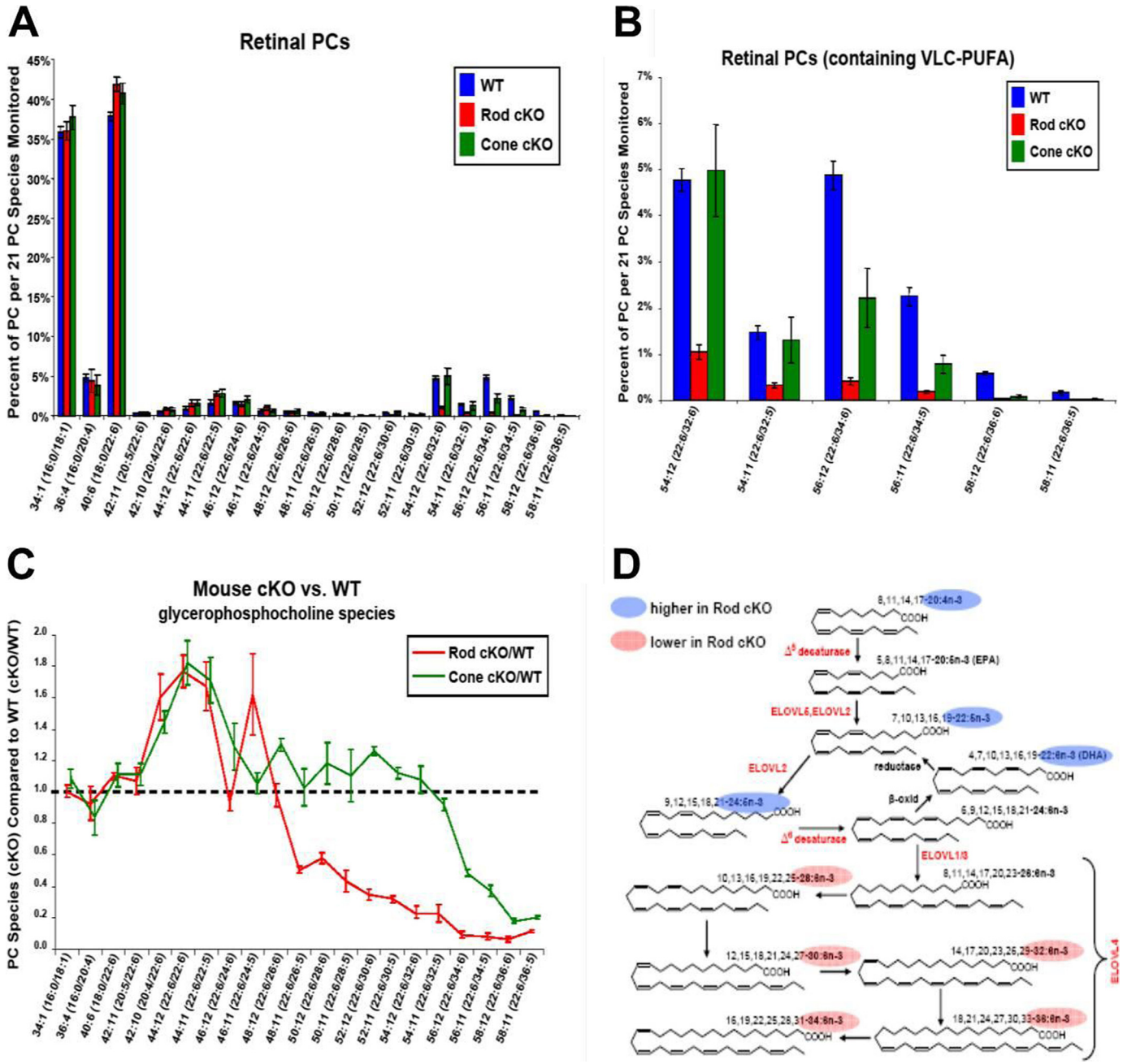

FIGURE 4. **Differential analysis of each PC species in retina of Rod- and Cone-cKO mice.** *A*, relative abundance of PC species observed in WT, Rod-cKO, and Cone-cKO mouse retinal extracts. *B*, greater detail of the region representing the PC species containing 32–36 VLC-PUFAs. *C*, graph showing the comparison of PC species observed in the retinal extracts of Rod- and Cone-cKO compared with WT mice (Rod-cKO is shown in *red*; Cone-cKO is shown in *green*). Note the *heavy dashed horizontal bar* indicating a ratio of 1. PC species located *above* this *line* indicate higher levels observed in cKO compared with WT; those located *below* indicate lower levels observed in cKO compared with WT. *D*, the VLC-PUFA synthesis pathway showing the species that were found to be higher in Rod-cKO mice compared with WT highlighted in *blue* and those that were found to be lower highlighted in *red*. Data shown are representative of six independent analyses (each retina from three mice). *Error bars* represent S.E.

ments in the Rod-cKO mutants (Fig. 6*C*) and the cone outer segments in the Cone-cKO mutants appeared normal for immersion-fixed mouse retinas. In the RPE of both Rod- and Cone-cKO retinas, an accumulation of lipid droplets was evident (Fig. 6, *E–G*); such droplets were only rarely observed in the RPE of normal control retinas (Fig. 6*D*). Lipofuscin-like granules were also observed in the RPE of the Cone- and especially the Rod-cKO retinas (Fig. 6, *E* and *F*); such granules were also evident in 15-month-old control retinas, although in the controls, they were clearly much less abundant.

Deterioration of Electrophysiological Responses in Conditional Knock-out Elovl4 Mice—ERG recordings were performed to assess retinal function in *Elovl4* Cone-cKO, *Elovl4* Rod-cKO, and WT adult mice (Fig. 5, *G–I*). For the Rod-cKO mice, we found a significant reduction in the maximum rod b-wave response (163 ± 19 microvolts (μV)) relative to WT (238 ± 18 μV) ($p = 0.011$) and a significant reduction in rod and cone mixed b-wave response (243 ± 16 μV) when compared with WT (316 ± 22 μV) ($p = 0.017$). Cone-cKO mice showed a significant reduction in flicker response (24 ± 4 μV) when

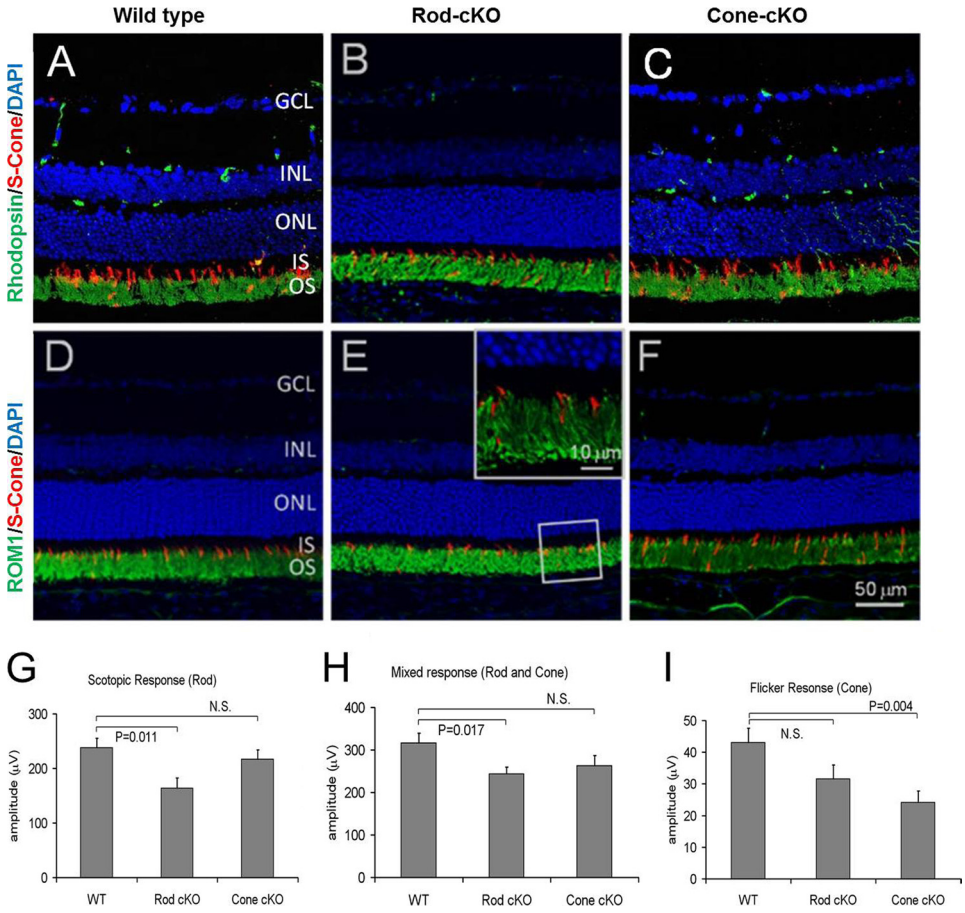

FIGURE 5. **Normal gross morphology of retina in Rod- or Cone-cKO mice with deterioration in photoreceptor-specific electrophysiological response.** Retinas from 3–5-month-old adult wild type (*A* and *D*), Rod-cKO (*B* and *E*), or Cone-cKO (*C* and *F*) mice were double fluorescence immunostained with Rhodopsin (*green*) and S-Cone (*red*; *A–C*) or ROM1 (*green*) and S-Cone (*red*; *D–F*). Nuclei were counterstained with DAPI. *Inset* in *E* shows a magnified image of the *boxed* area. *GCL*, ganglion cell layer; *INL*, inner nuclear layer; *ONL*, outer nuclear layer; *IS*, inner segment of photoreceptors; *OS*, outer segment of photoreceptors. *G–I*, ERG responses from C57B/6 WT control, *Elovl4* Rod-cKO, and *Elovl4* Cone-cKO mice. *G*, average maximum scotopic b-wave amplitudes to stimuli that elicit responses only from rods. *H*, average maximum mixed b-wave amplitudes to stimuli eliciting rod and cone responses. *I*, average maximum cone wave amplitudes in 10-Hz photopic flicker ERG. *Vertical axis* units are in μV. *N.S.*, not significant. *Error bars* represent S.E., $n = 11$ for wild type, $n = 18$ for Rod-cKO, and $n = 10$ for Cone-cKO.

compared with WT (43 ± 4 μV) ($p = 0.004$). The photoreceptor-specific pattern of reduction in the visual response recorded for cKO mice indicates that *Elovl4* is essential for the rod or cone photoreceptors to function properly in the retina. Additionally, the Rod-cKO mice demonstrate significant reductions in rod function, and the Cone-cKO mice demonstrate significant reductions in cone function.

DISCUSSION

Using photoreceptor-specific conditional knock-out mice, we provide evidence to implicate *Elovl4* as being essential for VLC-PUFA synthesis. In the current work, HPLC-MS analysis of retinal extracts from WT mice supports earlier studies (34), confirming that VLC-PUFA-containing glycerophospholipid species (C_{32}–C_{36}) are restricted almost entirely to the PCs with these VLC-PUFA PCs accounting for roughly 10% of the 21 PC species we monitored (Fig. 1, *C* and *D*). We also observed distribution profile differences when comparing these 21 monitored PC and PE species (Fig. 1*C*) and estimated the PC species to be ~5-fold higher in absolute abundance compared with the PE species.

The occurrence of VLC-PUFA acyl species contained in retinal glycerophospholipids was first observed over 20 years ago by Aveldaño (34). In agreement with the current work, this earlier study showed that the occurrence of VLC-PUFAs is restricted almost entirely to PC species found in the retina. Using a phospholipase A_2 enzyme, we also confirmed Aveldaño's (34) earlier work showing these VLC-PUFA acyl species were contained almost exclusively on the *sn*-1 position of these PCs with DHA (22:6*n*-3) occupying the *sn*-2 position. In the current study, we observed these VLC-PUFAs to be highly polyunsaturated, having mostly six double bonds, to a lesser extent five double bonds, and essentially no acyl chains with greater than six or fewer than five double bonds. Studies (22, 23, 26, 35) subsequent to that of Aveldaño (34) investigating retinal glycerophospholipids have for the most part used gas chromatography-mass spectrometry (GC-MS) methodology for analysis. Note that GC-MS analysis of glycerophospholipids requires the acyl fatty acids to be first deacylated from their corresponding glycerophospholipid precursor molecule, thus creating uncertainty as to their exact precursor molecule of origin. Once these fatty acids are deacylated and in "free form," they are

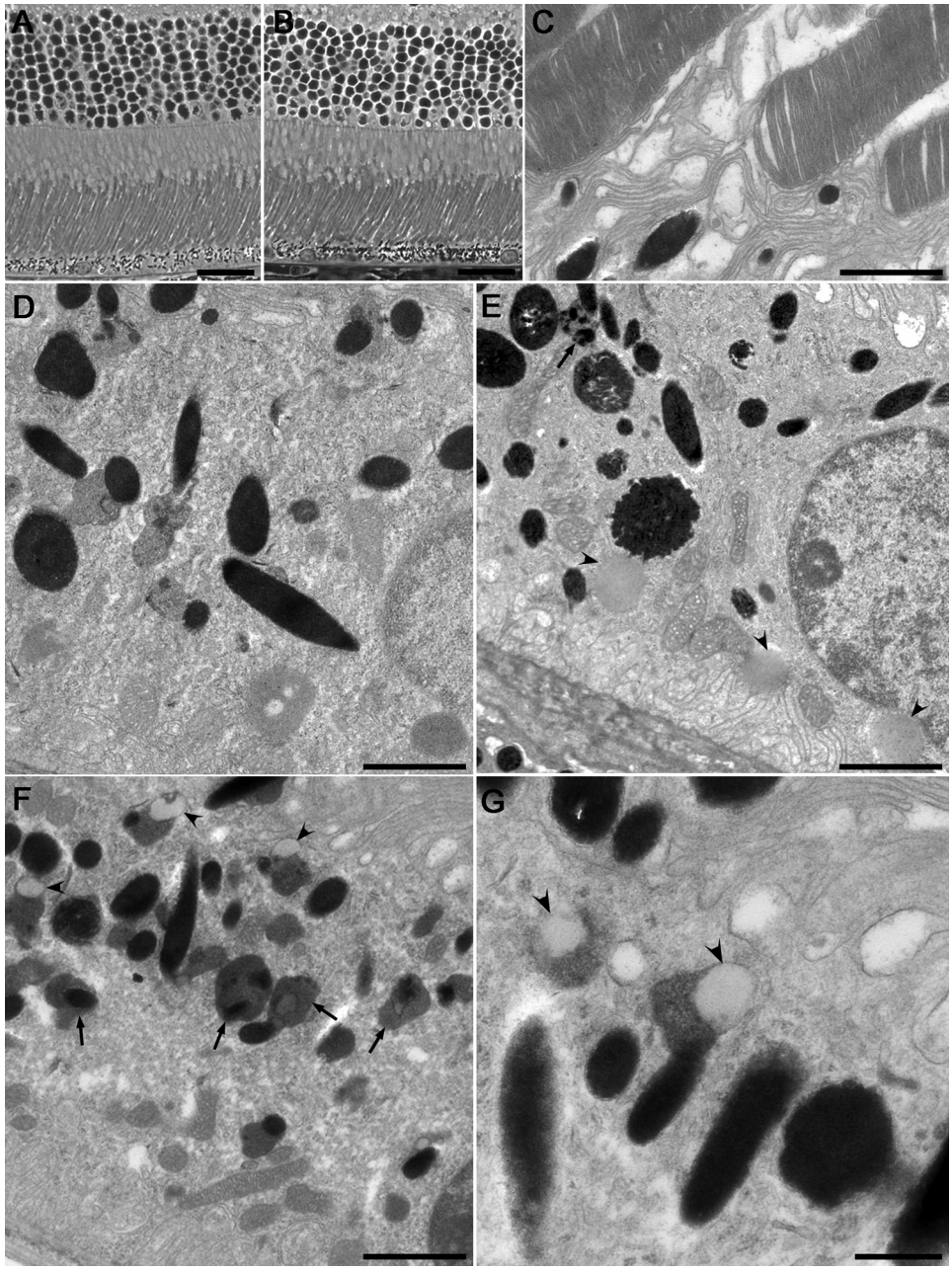

FIGURE 6. **Microscopy showing normal retinal morphology but abnormal accumulations of lipofuscin and lipid droplets in RPE.** Retinas from 15-month-old Rod- or Cone-cKO and wild type mice were studied. *A* and *B*, light micrographs of semithin sections from a control retina (*A*) and a Rod-cKO retina (*B*). Both sections are taken 0.5 mm from the optic nerved head. *Scale bars*, 20 μm. *C*, electron micrographs of the distal ends of rod outer segments from a Rod-cKO retina that was fixed by immersion; the disk membranes appear normal for this fixation procedure. *D–G*, electron micrographs of the RPE (apical surface, upper; basal surface, lower) from a control retina (*D*), a Cone-cKO retina (*E*), and a Rod-cKO retina (*F* and *G*). *Scale bars*, 1 μm (*C–F*) and 500 nm (*G*). Lipid droplets (*arrowheads*) are much more abundant in both the Rod- and Cone-cKO RPE. These retinas also contain somewhat more lipofuscin (*arrows*).

pooled for analysis, making it impossible to identify the specific glycerophospholipid from which they originated. A more recent study investigating retinal glycerophospholipids used HPLC directly coupled to the mass spectrometer operating in positive electrospray ionization mode, which allowed for the analysis of intact glycerophospholipids (37). In that study, retinal PCs were analyzed as protonated cations and collisionally induced dissociation fragmentation in the mass spectrometer of these cations yields only one detectable fragment ion: the phosphocholine headgroup with a mass-to-charge (m/z) ratio of 184. Additionally, the fragmentation of a protonated PE cation yields only one detectable fragment ion with a mass equal to the precursor ion less the mass of the PE headgroup (less than 141). Thus, the information provided indicates only the precursor ion mass and the specific glycerophospholipid class (PC or PE) to which it belongs, leaving uncertainty as to the exact identity of the specific acyl chains of the molecule.

An alternative mass spectrometric approach and the one used in the current work uses negative electrospray ionization to form anions (acetate anion adducts of PCs and deprotonated anions of PEs), which upon collisionally induced dissociation fragmentation produce intact acyl chain anion fragments,

allowing for a definitive characterization of the glycerophospholipid molecule (34). It is also noted that although in some cases the precise *sn*-1 and *sn*-2 positions of these glycerophospholipid acyl chains can be inferred by their relative fragment intensity ratios (38) this is not an exact rule, and numerous exceptions have been observed (38). We therefore used an $sPLA_2$ assay to confirm that the VLC-PUFAs are located on the *sn*-1 position of the retinal PCs. We also compared the retinal extracts of WT mice with those deficient in either cone or rod ELOVL4 (Cone-cKO or Rod-cKO) and observed both the Cone- and Rod-cKO mice to have increases in some of their intermediate length (C_{20}–C_{24}) PUFA-containing PCs, which are presumably precursors of the VLC-PUFAs as shown in Fig. 1*B*; a concomitant decrease in those PCs containing C_{28}–C_{36} (Rod-cKO) and C_{32}–C_{36} (cone-cKO) VLC-PUFAs; and closely similar amounts of the most abundant shorter acyl chain PCs (*e.g.* 16:0/18:1 and 18:0/22:6; Fig. 4, *A*–*C*). The more dramatic decrease in the VLC-PUFA PCs observed in the Rod-cKO compared with the Cone-cKO (Fig. 4*C*) is likely due to the 10–20-fold higher abundance of rod cells compared with cone cells in the retina, and note that the Cone-cKO mice still maintained ELOVL4-active rod cells, and the Rod-cKO mice still maintained ELOVL4-active cone cells. The higher abundance of the intermediate PC species, particularly the 20:4/22:6, 22:6/22:6, and 22:6/22:5 in the cKO mice compared with the WT may be due to a "backup" effect because these precursors were not further elongated to their VLC-PUFA products (Fig. 4*D*). Although these intermediate species only account for ~5% of the species monitored, it is possible that their higher abundance in the cKO mice could have some detrimental effect.

At present, the precise function of VLC-PUFA PCs in the retina remains largely unknown. They may perform a structural role in the lipid bilayer, such as forming a domain or rafts to facilitate protein interactions. The exclusive association of the phosphocholine headgroup and the *sn*-1 VLC-PUFA acyl chain may confer special properties to these unusual molecules in a lipid bilayer. For example, Agbaga *et al.* (23) proposed that the VLC-PUFA acyl chain may extend and cover the entire bilayer, thereby providing a flexible hinge at the rim location where the curvature of photoreceptor disk membranes is greatest. The abnormal accumulation of lipid droplets and lipofuscin granules observed in the RPE of mutant retinas may be related to defective retinoid mobility at the disk rim. Excessive lipofuscin in the RPE of *Abca4*−/− mice, a model for STGD1, appears to result from a lack of *N*-retinylidene-PE flippase activity of the ABCA4 protein in the disk membrane rims (39). Alternatively, it is possible that VLC-PUFAs perform a direct signaling function: Bazan *et al.* (40) have proposed that lipid molecules, such as DHA, serve as a special class of signaling molecules that activate specific receptors. Kahn-Kirby *et al.* (41) have reported that eicosapentaenoic acid and arachidonic acid can modulate transient receptor potential cation channel activity and modulate olfactory and nociceptive behavior.

At the light microscopy level, it appeared that the overall layered structure of the retina is not affected by the cell type-specific elimination of *Elovl4*. However, a closer examination of electron micrographs revealed some abnormalities in the RPE, including an excessive accumulation of lipofuscin and lipid droplets (Fig. 6). These accumulations may result from impaired digestion of photoreceptor disk membranes, which contain an altered balance of fatty acid precursors, due to the loss of ELOVL4.

Defects in our electrophysiological studies (ERGs) in *Elovl4* knock-out mice are consistent with its role in signal transduction. There are examples of genes whose loss of function affects ERGs but not morphology (42, 43). Alternatively, the lack of fatty acid elongation in ELOVL4 knock-out cells may affect multiple cellular processes, such as ER function, endocytosis, and secretion. The identification of the precise role these VLC-PUFA PCs play should prove informative to our understanding of retinal normal physiology and degeneration.

Lastly, we raise the question as to what possible mechanisms could be involved in the generation of these most unusual VLC-PUFA-containing glycerophospholipids found in the retina. Based on the revised pathway of Sprecher *et al.* (44), Fig. 1*B* shows that a combination of various desaturase and elongase enzymes is involved in their biosynthesis. Although plants and fungi have "lipid-linked" desaturases that are capable of acting on the intact acyl chains of glycerophospholipids substrates (45–47), desaturation and elongation of fatty acids in vertebrate systems requires an acyl-CoA substrate (48, 49) and the fatty acid to be free of any glycerophospholipid attachment. Because a number of desaturase and elongase reactions are required in coordinated and sequential steps to generate a VLC-PUFA from its initial precursor (*e.g.* 18:3*n*-3), it seems most likely that these reactions occur prior to any glycerophospholipid attachment, thus creating a varied yet highly regulated pool of fatty acids that are then methodically placed on the *sn*-1 position of the glycerophosphate destined to form the resulting PC through the action of specific acyltransferases.

In an alternative scheme, as the precocious, "waiting-to-be" VLC-PUFA journeys through its sequential desaturation/elongation steps, it is also possible that it can periodically be acylated to a glycerophosphocholine or lysoglycerophosphocholine to form a glycerophospholipid and hence is "off-limits" to desaturation/elongation during this time until once again it is deacylated and subjected to another round of desaturation/elongation. Because it is likely that both the desaturation/elongation steps and the acylation/deacylation steps occur in the endoplasmic reticulum, this scenario would not require the intermediate components to be constantly shuttled back and forth across organelles. However, more steps are involved in such a scheme compared with the alternative scheme described in the previous paragraph, so if it does indeed occur, then one would need to ask what advantages may be gained. It is also possible that the VLC-PUFAs are biosynthesized through either one or a combination of both schemes and then incorporated into "more typical," shorter acyl chain glycerophospholipid molecules through an acyl chain remodeling process (50, 51).

It is important to understand how VLC-PUFAs function at the molecular level to affect the functioning of the rods and cones. Our results show that the presence of some amount of PC containing a VLC-PUFA at the *sn*-1 position is essential for the visual process. Perhaps these special PCs play a biophysical role by their position in the lipid bilayer membrane, and their

lack is sufficient to distort its normal membrane structure or phase, thereby affecting the visual signal transduction process. Although we could not detect such structural affects in the microscopic imaging studies used in the current work, future retinal work involving newly developing imaging mass spectrometry (52, 53) may provide useful information for investigating the spatial and cellular distribution of glycerophospholipids containing VLC-PUFAs in individual rod and cone retinal cells and elucidation of their visual functions in health and disease.

Acknowledgments—We thank Kevin Wang and Bin Lin for technical assistance, Peter Shaw and other members of the Zhang laboratory for helpful discussions, and Dr. Yun Le and Gene Anderson for providing the cone- or rod-specific Cre mice. E.A.D. thanks Professor Michael H. Goldbaum at the University of California, San Diego Shiley Eye Center for special insight and help in understanding the pathophysiology and clinical implications of retinal disease.

REFERENCES

1. Kaplan, J., Bonneau, D., Frézal, J., Munnich, A., and Dufier, J. L. (1990) Clinical and genetic heterogeneity in retinitis pigmentosa. *Hum. Genet.* **85,** 635–642
2. Newsome, D. A. (1988) *Retinal Dystrophies and Degenerations*, pp. 135–159, Raven Press, New York
3. Stone, E. M., Nichols, B. E., Kimura, A. E., Weingeist, T. A., Drack, A., and Sheffield, V. C. (1994) Clinical features of a Stargardt-like dominant progressive macular dystrophy with genetic linkage to chromosome 6q. *Arch. Ophthalmol.* **112,** 765–772
4. Zhang, K., Kniazeva, M., Han, M., Li, W., Yu, Z., Yang, Z., Li, Y., Metzker, M. L., Allikmets, R., Zack, D. J., Kakuk, L. E., Lagali, P. S., Wong, P. W., MacDonald, I. M., Sieving, P. A., Figueroa, D. J., Austin, C. P., Gould, R. J., Ayyagari, R., and Petrukhin, K. (2001) A 5-bp deletion in ELOVL4 is associated with two related forms of autosomal dominant macular dystrophy. *Nat. Genet.* **27,** 89–93
5. Fox, B. G., Shanklin, J., Ai, J., Loehr, T. M., and Sanders-Loehr, J. (1994) Resonance Raman evidence for an Fe-O-Fe center in stearoyl-ACP desaturase. Primary sequence identity with other diiron-oxo proteins. *Biochemistry* **33,** 12776–12786
6. Shanklin, J., Whittle, E., and Fox, B. G. (1994) Eight histidine residues are catalytically essential in a membrane-associated iron enzyme, stearoyl-CoA desaturase, and are conserved in alkane hydroxylase and xylene monooxygenase. *Biochemistry* **33,** 12787–12794
7. Jackson, M. R., Nilsson, T., and Peterson, P. A. (1990) Identification of a consensus motif for retention of transmembrane proteins in the endoplasmic reticulum. *EMBO J.* **9,** 3153–3162
8. Jackson, M. R., Nilsson, T., and Peterson, P. A. (1993) Retrieval of transmembrane proteins to the endoplasmic reticulum. *J. Cell Biol.* **121,** 317–333
9. Schröder, S., Schimmöller, F., Singer-Krüger, B., and Riezman, H. (1995) The Golgi-localization of yeast Emp47p depends on its di-lysine motif but is not affected by the ret1–1 mutation in α-COP. *J. Cell Biol.* **131,** 895–912
10. Maugeri, A., Meire, F., Hoyng, C. B., Vink, C., Van Regemorter, N., Karan, G., Yang, Z., Cremers, F. P., and Zhang, K. (2004) A novel mutation in the ELOVL4 gene causes autosomal dominant Stargardt-like macular dystrophy. *Invest. Ophthalmol. Vis. Sci.* **45,** 4263–4267
11. Bernstein, P. S., Tammur, J., Singh, N., Hutchinson, A., Dixon, M., Pappas, C. M., Zabriskie, N. A., Zhang, K., Petrukhin, K., Leppert, M., and Allikmets, R. (2001) Diverse macular dystrophy phenotype caused by a novel complex mutation in the ELOVL4 gene. *Invest. Ophthalmol. Vis. Sci.* **42,** 3331–3336
12. Cinti, D. L., Cook, L., Nagi, M. N., and Suneja, S. K. (1992) The fatty acid chain elongation system of mammalian endoplasmic reticulum. *Prog. Lipid Res.* **31,** 1–51
13. Karan, G., Yang, Z., Howes, K., Zhao, Y., Chen, Y., Cameron, D. J., Lin, Y., Pearson, E., and Zhang, K. (2005) Loss of ER retention and sequestration of the wild-type ELOVL4 by Stargardt disease dominant negative mutants. *Mol. Vis.* **11,** 657–664
14. Grayson, C., and Molday, R. S. (2005) Dominant negative mechanism underlies autosomal dominant Stargardt-like macular dystrophy linked to mutations in ELOVL4. *J. Biol. Chem.* **280,** 32521–32530
15. Vasireddy, V., Vijayasarathy, C., Huang, J., Wang, X. F., Jablonski, M. M., Petty, H. R., Sieving, P. A., and Ayyagari, R. (2005) Stargardt-like macular dystrophy protein ELOVL4 exerts a dominant negative effect by recruiting wild-type protein into aggresomes. *Mol. Vis.* **11,** 665–676
16. Oh, C. S., Toke, D. A., Mandala, S., and Martin, C. E. (1997) ELO2 and ELO3, homologues of the *Saccharomyces cerevisiae* ELO1 gene, function in fatty acid elongation and are required for sphingolipid formation. *J. Biol. Chem.* **272,** 17376–17384
17. Jakobsson, A., Westerberg, R., and Jacobsson, A. (2006) Fatty acid elongases in mammals: their regulation and roles in metabolism. *Prog. Lipid Res.* **45,** 237–249
18. Agbaga, M. P., Mandal, M. N., and Anderson, R. E. (2010) Retinal very long-chain PUFAs: new insights from studies on ELOVL4 protein. *J. Lipid Res.* **51,** 1624–1642
19. Edwards, A. O., Donoso, L. A., and Ritter, R., 3rd (2001) A novel gene for autosomal dominant Stargardt-like macular dystrophy with homology to the SUR4 protein family. *Invest. Ophthalmol. Vis. Sci.* **42,** 2652–2663
20. Tvrdik, P., Westerberg, R., Silve, S., Asadi, A., Jakobsson, A., Cannon, B., Loison, G., and Jacobsson, A. (2000) Role of a new mammalian gene family in the biosynthesis of very long chain fatty acids and sphingolipids. *J. Cell Biol.* **149,** 707–718
21. Zhang, X. M., Yang, Z., Karan, G., Hashimoto, T., Baehr, W., Yang, X. J., and Zhang, K. (2003) Elovl4 mRNA distribution in the developing mouse retina and phylogenetic conservation of Elovl4 genes. *Mol. Vis.* **9,** 301–307
22. Cameron, D. J., Tong, Z., Yang, Z., Kaminoh, J., Kamiyah, S., Chen, H., Zeng, J., Chen, Y., Luo, L., and Zhang, K. (2007) Essential role of Elovl4 in very long chain fatty acid synthesis, skin permeability barrier function, and neonatal survival. *Int. J. Biol. Sci.* **3,** 111–119
23. Agbaga, M. P., Brush, R. S., Mandal, M. N., Henry, K., Elliott, M. H., and Anderson, R. E. (2008) Role of Stargardt-3 macular dystrophy protein (ELOVL4) in the biosynthesis of very long chain fatty acids. *Proc. Natl. Acad. Sci. U.S.A.* **105,** 12843–12848
24. Mandal, M. N., Ambasudhan, R., Wong, P. W., Gage, P. J., Sieving, P. A., and Ayyagari, R. (2004) Characterization of mouse orthologue of ELOVL4: genomic organization and spatial and temporal expression. *Genomics* **83,** 626–635
25. Rezanka, T. (1989) Very-long-chain fatty acids from the animal and plant kingdoms. *Prog. Lipid Res.* **28,** 147–187
26. Liu, A., Chang, J., Lin, Y., Shen, Z., and Bernstein, P. S. (2010) Long-chain and very long-chain polyunsaturated fatty acids in ocular aging and age-related macular degeneration. *J. Lipid Res.* **51,** 3217–3229
27. McMahon, A., Butovich, I. A., and Kedzierski, W. (2011) Epidermal expression of an Elovl4 transgene rescues neonatal lethality of homozygous Stargardt disease-3 mice. *J. Lipid Res.* **52,** 1128–1138
28. Adams, D. J., Quail, M. A., Cox, T., van der Weyden, L., Gorick, B. D., Su, Q., Chan, W. I., Davies, R., Bonfield, J. K., Law, F., Humphray, S., Plumb, B., Liu, P., Rogers, J., and Bradley, A. (2005) A genome-wide, end-sequenced 129Sv BAC library resource for targeting vector construction. *Genomics* **86,** 753–758
29. Le, Y. Z., Ash, J. D., Al-Ubaidi, M. R., Chen, Y., Ma, J. X., and Anderson, R. E. (2004) Targeted expression of Cre recombinase to cone photoreceptors in transgenic mice. *Mol. Vis.* **10,** 1011–1018
30. Le, Y. Z., Zheng, L., Zheng, W., Ash, J. D., Agbaga, M. P., Zhu, M., and Anderson, R. E. (2006) Mouse opsin promoter-directed Cre recombinase expression in transgenic mice. *Mol. Vis.* **12,** 389–398
31. Kokotos, G., Hsu, Y. H., Burke, J. E., Baskakis, C., Kokotos, C. G., Magrioti, V., and Dennis, E. A. (2010) Potent and selective fluoroketone inhibitors of group VIA calcium-independent phospholipase A2. *J. Med. Chem.* **53,** 3602–3610
32. Lucas, K. K., and Dennis, E. A. (2005) Distinguishing phospholipase A2 types in biological samples by employing group-specific assays in the presence of inhibitors. *Prostaglandins Other Lipid Mediat.* **77,** 235–248

33. Hazlett, T. L., and Dennis, E. A. (1985) Affinity chromatography of phospholipase A2 from *Naja naja naja* (Indian cobra) venom. *Toxicon* **23,** 457–466
34. Aveldaño, M. I. (1988) Phospholipid species containing long and very long polyenoic fatty acids remain with rhodopsin after hexane extraction of photoreceptor membranes. *Biochemistry* **27,** 1229–1239
35. Suh, M., and Clandinin, M. T. (2005) 20:5n-3 but not 22:6n-3 is a preferred substrate for synthesis of n-3 very-long- chain fatty acids (C24–C36) in retina. *Curr. Eye Res.* **30,** 959–968
36. Dennis, E. A., Cao, J., Hsu Y. H., Magrioti V., and Kokotos, G. (2011) Phospholipase A2 enzymes: physical structure, biological function, disease implication, chemical inhibition, and therapeutic intervention. *Chem. Rev.* **111,** 6130–6185
37. McMahon, A., Jackson, S. N., Woods, A. S., and Kedzierski, W. (2007) A Stargardt disease-3 mutation in the mouse Elovl4 gene causes retinal deficiency of C32–C36 acyl phosphatidylcholines. *FEBS Lett.* **581,** 5459–5463
38. Boon, C. J., Klevering, B. J., Cremers, F. P., Zonneveld-Vrieling, M. N., Theelen, T., Den Hollander, A. I., and Hoyng, C. B. (2009) Central areolar choroidal dystrophy. *Ophthalmology* **116,** 771–782, 782.e1
39. Weng, J., Mata, N. L., Azarian, S. M., Tzekov, R. T., Birch, D. G., and Travis, G. H. (1999) Insights into the function of Rim protein in photoreceptors and etiology of Stargardt's disease from the phenotype in abcr knockout mice. *Cell* **98,** 13–23
40. Bazan, N. G., Calandria, J. M., and Serhan, C. N. (2010) Rescue and repair during photoreceptor cell renewal mediated by docosahexaenoic acid-derived neuroprotectin D1. *J. Lipid Res.* **51,** 2018–2031
41. Kahn-Kirby, A. H., Dantzker, J. L., Apicella, A. J., Schafer, W. R., Browse, J., Bargmann, C. I., and Watts, J. L. (2004) Specific polyunsaturated fatty acids drive TRPV-dependent sensory signaling *in vivo*. *Cell* **119,** 889–900
42. Hattar, S., Lucas, R. J., Mrosovsky, N., Thompson, S., Douglas, R. H., Hankins, M. W., Lem, J., Biel, M., Hofmann, F., Foster, R. G., and Yau, K. W. (2003) Melanopsin and rod-cone photoreceptive systems account for all major accessory visual functions in mice. *Nature* **424,** 76–81
43. Libby, R. T., Kitamoto, J., Holme, R. H., Williams, D. S., and Steel, K. P. (2003) Cdh23 mutations in the mouse are associated with retinal dysfunction but not retinal degeneration. *Exp. Eye. Res.* **77,** 731–739
44. Sprecher, H., Luthria, D. L., Mohammed, B. S., and Baykousheva, S. P. (1995) Reevaluation of the pathways for the biosynthesis of polyunsaturated fatty acids. *J. Lipid Res.* **36,** 2471–2477
45. Galle-Le Bastard, A. M., Demandre, C., Oursel, A., Mazliak, P., and Kader, J. C. (2000) Phosphatidylcholine molecular species involved in Γ-linolenic acid giosynthesis in microsomes from borage seeds. *Physiol. Plant.* **108,** 118–124
46. Griffiths, G., Stobart, A. K., and Stymne, S. (1988) Δ6- and Δ12-desaturase activities and phosphatidic acid formation in microsomal preparations from the developing cotyledons of common borage (*Borago officinalis*). *Biochem. J.* **252,** 641–647
47. Jackson, F. M., Fraser, T. C., Smith, M. A., Lazarus, C., Stobart, A. K., and Griffiths, G. (1998) Biosynthesis of C18 polyunsaturated fatty acids in microsomal membrane preparations from the filamentous fungus *Mucor circinelloides*. *Eur. J. Biochem.* **252,** 513–519
48. Sprecher, H. (1999) An update on the pathways of polyunsaturated fatty acid metabolism. *Curr. Opin. Clin. Nutr. Metab. Care* **2,** 135–138
49. Okayasu, T., Nagao, M., Ishibashi, T., and Imai, Y. (1981) Purification and partial characterization of linoleoyl-CoA desaturase from rat liver microsomes. *Arch. Biochem. Biophys.* **206,** 21–28
50. Lands, W. E. (2000) Stories about acyl chains. *Biochim. Biophys. Acta* **1483,** 1–14
51. Yamashita, A., Sugiura, T., and Waku, K. (1997) Acyltransferases and transacylases involved in fatty acid remodeling of phospholipids and metabolism of bioactive lipids in mammalian cells. *J. Biochem.* **122,** 1–16
52. Murphy, R. C., Hankin, J. A., and Barkley, R. M. (2009) Imaging of lipid species by MALDI mass spectrometry. *J. Lipid Res.* **50, (**suppl.) S317–S322
53. Harkewicz, R., and Dennis, E. A. (2011) Applications of mass spectrometry to lipids and membranes. *Annu. Rev. Biochem.* **80,** 301–325